Applied Physics Letters

RESEARCH ARTICLE | JULY 01 2024

Strained single crystal high entropy oxide manganite thin films

Special Collection: Era of Entropy: Synthesis, Structure, Properties, and Applications of High-Entropy Materials

Zhibo Zhao ; Moaz Waqar ; Arun Kumar Jaiswal ; Aaditya Rangan Raghavan ; Dirk Fuchs ; Jing Lin ; Torsten Brezesinski ; Subramshu S. Bhattacharya ; Horst Hahn ; Xiaoqing Pan ; Robert Kruk ; Abhishek Sarkar

Appl. Phys. Lett. 125, 011902 (2024)
https://doi.org/10.1063/5.0206767
CHORUS

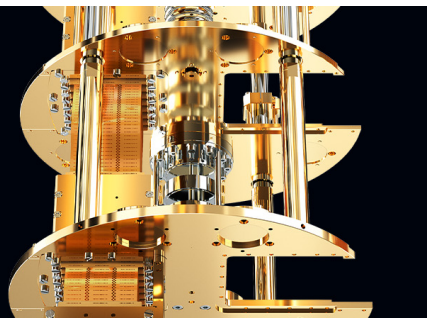

AIP Publishing

Applied Physics Letters ARTICLE pubs.aip.org/aip/apl

Strained single crystal high entropy oxide manganite thin films

Cite as: Appl. Phys. Lett. **125**, 011902 (2024); doi: 10.1063/5.0206767
Submitted: 4 March 2024 · Accepted: 12 June 2024 ·
Published Online: 1 July 2024

View Online Export Citation CrossMark

Zhibo Zhao,[1,2] Moaz Waqar,[3] Arun Kumar Jaiswal,[4] Aaditya Rangan Raghavan,[5] Dirk Fuchs,[4] Jing Lin,[1] Torsten Brezesinski,[1] Subramshu S. Bhattacharya,[5] Horst Hahn,[1,2,6] Xiaoqing Pan,[3,7,8] Robert Kruk,[1] and Abhishek Sarkar[1,2,9,a)]

AFFILIATIONS

[1]Karlsruhe Institute of Technology, Institute of Nanotechnology, Kaiserstr. 12, 76131 Karlsruhe, Germany
[2]KIT-TUD-Joint Research Laboratory Nanomaterials, Technical University Darmstadt, 64287 Darmstadt, Germany
[3]Department of Materials Science and Engineering, University of California, Irvine, California 92697, USA
[4]Karlsruhe Institute of Technology, Institute for Quantum Materials and Technologies, Kaiserstr. 12, 76131 Karlsruhe, Germany
[5]Nanofunctional Materials Technology Centre (NFMTC), Department of Metallurgical and Materials Engineering, Indian Institute of Technology Madras, Chennai 600036, India
[6]School of Sustainable Chemical, Biological and Materials Engineering, The University of Oklahoma, Norman, Oklahoma 73019, USA
[7]Department of Physics and Astronomy, University of California, Irvine, California 92697, USA
[8]Irvine Materials Research Institute, University of California, Irvine, California 92697, USA
[9]Department of Materials Science and Engineering, Indian Institute of Technology Delhi, Hauz Khas, New Delhi 110016, India

Note: This paper is part of the APL Special Collection on Era of Entropy: Synthesis, Structure, Properties, and Applications of High Entropy Materials.

[a)]**Author to whom correspondence should be addressed:** abhishek.sarkar@kit.edu and asarkar@iitd.ac.in

ABSTRACT

The ability to accommodate multiple principal cations within a single crystallographic structure makes high entropy oxides (HEOs) ideal systems for exploring new composition–property relationships. In this work, the high-entropy design strategy is extended to strained single-crystal HEO-manganite (HEO-Mn) thin films. Phase-pure orthorhombic films of $(Gd_{0.2}La_{0.2}Nd_{0.2}Sm_{0.2}Sr_{0.2})MnO_3$ were deposited on three different single-crystal substrates: $SrTiO_3$ (STO) (100), $NdGaO_3$ (110), and $LaAlO_3$ (LAO) (100), each inducing different degrees of epitaxial strain. Fully coherent growth of the thin films is observed in all cases, despite the high degree of lattice mismatch between HEO-Mn and LAO. Magnetometry measurements reveal distinct differences in the magnetic properties between epitaxially strained HEO-Mn thin films and their bulk crystalline HEO counterparts. In particular, the bulk polycrystalline HEO-Mn shows two magnetic transitions as opposed to a single one observed in epitaxial thin films. Moreover, the HEO-Mn film deposited on LAO exhibits a significant reduction in the Curie temperature, which is attributed to the strong variation of the *in-plane* lattice parameter along the thickness of the film and the resulting changes in the Mn–O–Mn bond geometry. Thus, this preliminary study demonstrates the potential of combining high entropy design with strain engineering to tailor the structure and functionality of perovskite manganites.

High entropy oxides (HEOs) represent a rapidly emerging class of functional materials, which has attracted considerable research interest over the past few years.[1–3] A notable strength of HEOs lies in their remarkable capacity to maintain phase-purity despite accommodating multiple principal cations in a single sublattice, thereby offering an expansive compositional space for exploring opportunities to tailor properties.[1–3] The realm of HEOs already encompasses diverse oxide classes and compositions, such as transition metal (TM)-based rock salt, TM-based spinels, rare-earth (RE)-based fluorite, RE-TM-based perovskite, etc.[4–6] As a result, numerous functionalities, for instance, electrochemical cyclic stability, catalytic activity, thermal insulation, narrow bandgap, etc., have been reported for different HEOs.[7–13]

The magnetic phase separation phenomenon observed in crystallographic single-phase systems is an occurrence common to several classes of HEOs.[14–16] This phenomenon arises from the presence of many different metal cations, each with different valence states, spin states, and radii, within a single sub-lattice of HEOs. Among other consequences, this results in different metal–oxygen–metal (M–O–M) bond distances and angles.[17,18] Thus, the magnetic exchange interactions, influenced by the M–O–M bond geometry and the specific types of metal cations, exhibit strong local variations. This leads to a complex magneto-electronic free-energy landscape in HEOs, determined by competing magnetic states, often resulting in magnetic phase separation.[17] In a recent study, the consequences of such magnetic phase separation were observed in perovskite-type HEO manganites (Gd,La,Nd,Sm)$_{1-x}$Sr$_x$MnO$_3$, including the enhancement of colossal magnetoresistance and the occurrence of dual magnetic transitions.[19] Standard hole-doping by varying the amount of Sr was utilized to control the structure and magneto-electronic phase-space of HEO-manganites.[19] In this study, we use an external stimulus, specifically substrate-induced epitaxial strain, to manipulate both the structure and magnetic properties of thin films of HEO-manganites.

Epitaxial films of $(Gd_{0.2}La_{0.2}Nd_{0.2}Sm_{0.2}Sr_{0.2})MnO_3$, henceforth referred to as HEO-Mn, were deposited utilizing pulsed laser deposition (PLD) on three different single crystal substrates: $LaAlO_3$ (LAO), $NdGaO_3$ (NGO), and $SrTiO_3$ (STO). These specific substrates, each with varying lattice parameters, were selected to induce different types of epitaxial strains. Throughout the manuscript, the lattice parameter values are consistently presented in terms of their pseudo-cubic equivalence (a_{pc}) to facilitate a direct comparison between films deposited on orthorhombic and cubic substrates. The a_{pc} of orthorhombic bulk HEO-Mn is 3.875 Å, while that of STO, NGO, and LAO substrates is 3.90, 3.86, and 3.79 Å, respectively. Figure 1(a) represents the degree of lattice mismatch (*in-plane*) between the substrates and bulk HEO-Mn. Keeping in mind the relationship between cubic and orthorhombic structures, crystals of (100) orientation were used for cubic LAO and STO substrates, while (110) orientation was used for the orthorhombic NGO substrate. The thin films on different substrates were deposited simultaneously to ensure identical growth conditions crucial for comparison. Detailed investigations have been performed to evaluate the strain states and distinct structural features at the interfaces. The results of magnetometry measurements underline prominent strain-driven changes in the magnetic transition of HEO-Mn. Experimental details are provided in the supplementary information.

The global structure and surface morphology information of HEO-Mn on various substrates, obtained from high-resolution x-ray diffraction (XRD), x-ray reflectometry (XRR), and atomic force microscopy (AFM), are provided in Figs. 1(b) and 1(g). Figure 1(b) along with the full range $\theta-2\theta$ XRD scans (Fig. S1) indicates epitaxial growth of the HEO-Mn films on the respective single crystalline substrates. The differences in the *out-of-plane* (OOP) XRD peak positions [Fig. 1(b)] between the films represent the different degrees of substrate induced strain. In the case of HEO-Mn deposited on LAO, a shift in the XRD peak toward the lower angle [in Fig. 1(b)] represents a considerable elongation of the OOP lattice parameter and an accompanying in-plane (IP) compressive strain. Conversely, the smaller OOP lattice parameter in the case of STO indicates IP tensile strain. The negligible difference between the bulk HEO-Mn and film peak

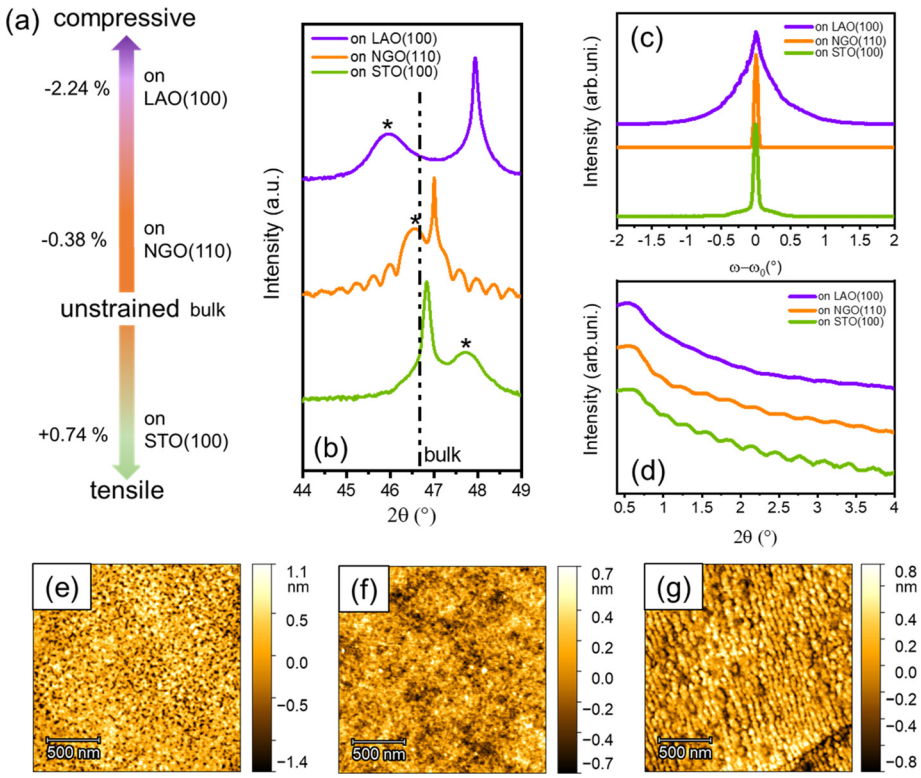

FIG. 1. (a) Schematic of lattice mismatch between HEO-Mn and the underlying substrates (*in-plane*). (b) XRD indicating the phase purity of HEO-Mn thin films deposited on various substrates, LAO (100), NGO (110), and STO (100). The asterisk marks represent the film peaks. (c) ω-scan of HEO-Mn deposited on various substrates. (d) XRR of HEO-Mn deposited on various substrates confirming the thickness of 25 nm. (e)–(g) AFM images indicating the smooth surfaces of HEO-Mn (with root mean square roughness below 0.33 nm) deposited on LAO, NGO, and STO, respectively.

positions highlights the small degree of OOP strain induced in the case of NGO. Additionally, the clear thickness oscillations observed in the XRD pattern [Fig. 1(a)] highlight the superior epitaxial quality of the film deposited on NGO. The thickness of the HEO-Mn films is around 25 nm, as estimated from the periodic oscillations as observed in XRR, Fig. 1(c). Rocking curve measurements (ω-scans) are performed to further evaluate the strain states in the HEO-Mn films, Fig. 1(d). The ω-scans of HEO-Mn deposited on LAO exhibit the broadest full width of half maximum (FWHM) of 0.427°. This highlights the relaxation and mosaic nature of the HEO-Mn deposited on LAO, which is underpinned by the high degree of lattice mismatch. Films on STO and NGO show narrow FWHM of 0.068° and 0.058°, respectively, indicating their good crystalline quality. Apart from the strain influenced global structure of HEO-Mn, the strain related surface morphology has been investigated using AFM. In general, all the HEO thin films exhibit smooth surface morphology with a root mean square surface roughness (R_a) of less than 0.5 nm. The smallest lattice mismatch and, correspondingly, the lowest epitaxial strain in the case of HEO-Mn film deposited on NGO results in a significantly smoother surface with $R_a = 0.171$ nm. On the other hand, the films deposited on LAO and STO show $R_a = 0.330$ nm and $R_a = 0.223$ nm, respectively. HEO-Mn on STO also featured atomically flat terraces separated by periodic steps as anticipated after etching treatment of the STO substrate.

The x-ray reciprocal space mapping (RSM) measurements (Fig. 2) were performed in order to assess the coherence of the HEO-Mn films with the underlying substrate and the accompanying strains (IP: ε_{xx} and OOP: ε_{zz}) in the films. The RSM measurements were performed in the vicinity of the asymmetric (204) Bragg reflection of cubic LAO and STO, while (332) was used for the orthorhombic NGO. The large compressive strain due to the significant lattice mismatch and the resulting relaxation in the case of the LAO substrate is evident from the large difference in the q_z value along with the lack of proper vertical alignment (difference in the q_x value) between the film and substrate reflections. The ε_{xx} and ε_{zz} in the case of the HEO-Mn/LAO film are −1.31% and +2.05%, respectively. Conversely, in the case of the NGO substrate, a perfect vertical alignment between the (332) substrate and the film peak is observed with a small difference in the q_z value. This indicates high epitaxial quality and no sign of strain relaxation. Consequently, a small degree of IP compressive strain is induced in the films deposited on NGO, with $\varepsilon_{xx} = -0.36\%$ and $\varepsilon_{zz} = 0.52\%$. In

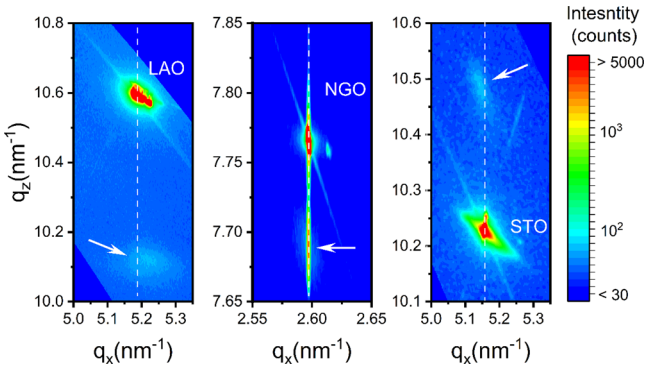

FIG. 2. RSM of HEO-Mn on different substrates: LAO, NGO, and STO. Arrows denote the diffraction peaks of HEO-Mn thin films. Intensity is presented in logarithmic scale.

the case of films deposited on STO, the difference in the q_x value, although small, indicates certain degree of IP mismatch and relaxation. The q_z value of the film is larger than that of the STO substrate, confirming the IP tensile strain and accompanying OOP compression. The corresponding ε_{xx} and ε_{zz} in this case are +0.20% and −1.52%, respectively. The Poisson ratio (ν) of the thin films can be roughly estimated using $\nu = \varepsilon_{zz}/(\varepsilon_{zz} - 2\,\varepsilon_{xx})$. The ν of HEO-Mn thin films ranges from 0.4 to 0.8. ν is highest in the case of STO, which is well above the range of 0.3–0.5 typically observed in the perovskite oxides.[20,21]

Atomic-scale scanning transmission electron microscopy (STEM) with energy-dispersive x-ray spectroscopy (EDS) was used to gain insight into the local structure, especially at the film-substrate interface. Given the superior quality of the HEO-Mn film deposited on NGO and the large compressive strain induced by LAO resulting from the large lattice mismatch, these systems were selected for further investigation using STEM. The STEM results for the HEO-Mn film grown on NGO are shown in Fig. 3, while those for LAO are presented in Fig. S2. High-angle annular dark-field (HAADF) STEM images of the HEO-Mn film deposited on NGO [Fig. 3(a)] and LAO (Fig. S2) show excellent crystallinity with fully coherent interface between film and the substrate, which is in good agreement with the XRD results. Notably, despite the large lattice mismatch and relaxation observed from RSM, the film grown on LAO is fully coherent without any presence of misfit dislocations. This proves the superior ability of HEO-Mn films for accommodating high degree of elastic strain without any formation of dislocations. The fast Fourier transforms (FFTs) of the HAADF images (shown in the insets) confirm the orthorhombic phase in both films. EDS maps of HEO-Mn film deposited on NGO [Fig. 3(b)] as well as LAO (Fig. S2) confirm the nanoscopic elemental homogeneity without any observable chemical segregation throughout the thin film.

To fully understand the evolution of strain across the thickness of the films, both IP and OOP lattice parameters (a_{pc}) were calculated from the atomic-scale HAADF images, which are presented in Fig. 4. Significant differences can be observed in the variation of the IP a_{pc} with the thickness of the deposited film. The results confirm the high compressive strain in the HEO-Mn film on LAO (compared to that of NGO) showing a smaller IP a_{pc} of around 3.79 Å (compared to 3.86 Å on NGO). In the case of HEO-Mn deposited on NGO, the IP a_{pc} remains largely constant throughout the thickness. In contrast, the IP a_{pc} of the film deposited on the LAO substrate gradually increases up to 10-unit cells, then decreases up to 15-unit cells, and finally levels off. This variation of the IP a_{pc} across the thickness in the case of LAO is intriguing and provides a plausible mechanism by which the system accommodates a substantial amount of epitaxial strain without exhibiting apparent interfacial mismatches. Such variation of the IP a_{pc} across the thickness can also account for the pronounced mosaicity of the sample deposited on LAO, as indicated by the large FWHM in the ω-scans [Fig. 1(d)].

The applied epitaxial strain is known to have a profound effect on the magnetic properties of manganite perovskites due to the strain-induced change in the Mn–O–Mn bond geometry.[22,23] Consequently, temperature (M-T) and external magnetic field (M-H) dependent magnetization measurements were performed. Figure 5 represents the *in-plane* field cooled (FC) part of the M–T plots. Figure S3 presents the *in-plane* M-H data taken at different temperatures along with the *out-of-plane* M-H taken at 5 K. HEO-Mn thin films, irrespective of the underlying substrates and strain states, exhibit a single magnetic

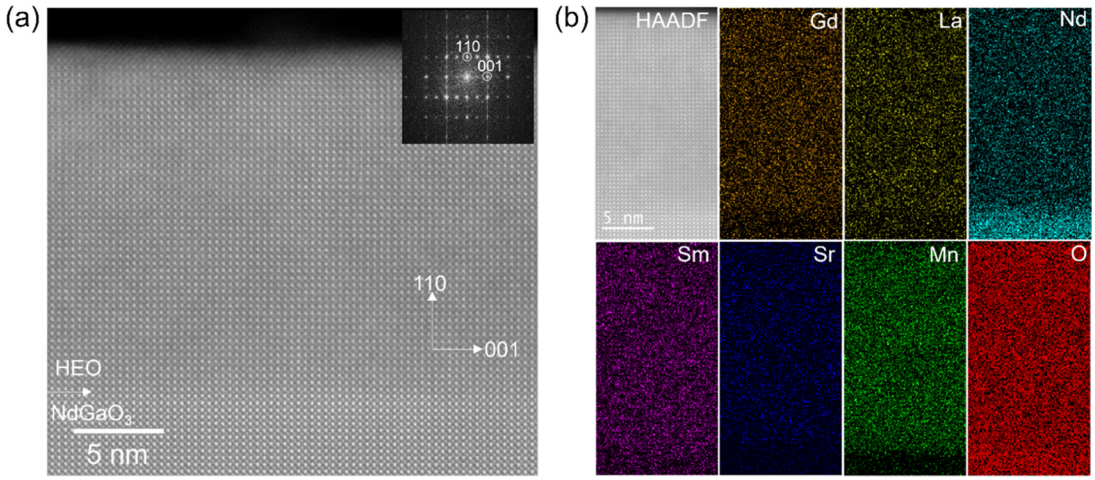

FIG. 3. STEM analysis of HEO-Mn film on NGO (110) substrate. (a) High-resolution HAADF-STEM image showing the epitaxial growth of HEO-Mn thin film on NGO. The fast Fourier transform (FFT) in the inset showcases the orthorhombic nature of the HEO-Mn film. (b) HAADF image and elemental distribution maps confirming the homogeneous distribution of the constituent elements in the HEO-Mn film.

transition. However, the transition temperature varies as a function of the straining. The corresponding low temperature M–H data for HEO-Mn deposited on LAO and STO are shown in Fig. S3, which ascertain the ferromagnetic ground state of the thin films. It should be noted that the M-H measurement of HEO-Mn deposited on NGO (not shown here) is dominated by the strong paramagnetic behavior of the NGO substrate, which limits precise estimation of the saturated magnetic moment (M_S) per formula unit (*f.u.*) of the sample; nevertheless, the ferromagnetic ground state can be unambiguously confirmed by the presence of the hysteresis loop.

To begin the discussion of the M–T data, we first refer to the magnetic properties observed for the bulk polycrystalline HEO-Mn counterparts.[19] Indeed, all of the thin films studied here exhibit a single transition temperature, in contrast to the two transition temperatures (143 and 105 K) observed for the bulk polycrystalline counterparts.[19] The two magnetic transitions observed in the bulk HEO-Mn were presumed to arise from the magneto-electronic phase separation, which was promoted by the local A-site cation disorder.[19] The presence of multiple A-site cation with different ionic radii creates a non-uniform environment around the Mn–O–Mn resulting in locally fluctuating Mn–O–Mn bond angle.[17–19] On the one hand, the prevailing magnetic state and the subsequent transition temperature in HEO-Mn are primarily determined by the average Mn–O–Mn bond angle, but at the same time, the locally distorted Mn–O–Mn bonds facilitate the gradual onset of magnetic ordering within a finite and measurable temperature range. Based on this paradigm, it is interpreted that 143 K is the onset of short-range correlation effects in the bulk where the magnetically ordered phase coexists with a paramagnetic phase. This process extends over 40 K, leading to the robust transition to the ground

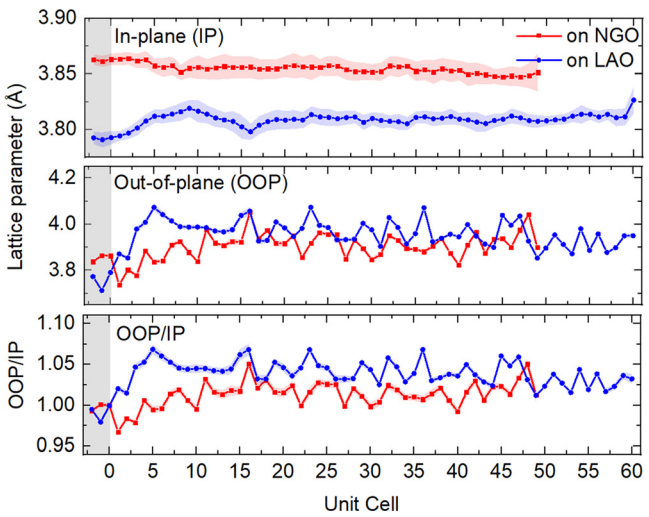

FIG. 4. Variation of the *in-plane* (IP) and *out-of-plane* (OOP) lattice parameters along the thickness of HEO-Mn films deposited on NGO and LAO, as obtained from STEM images. The faded region around the curves shows the standard deviation.

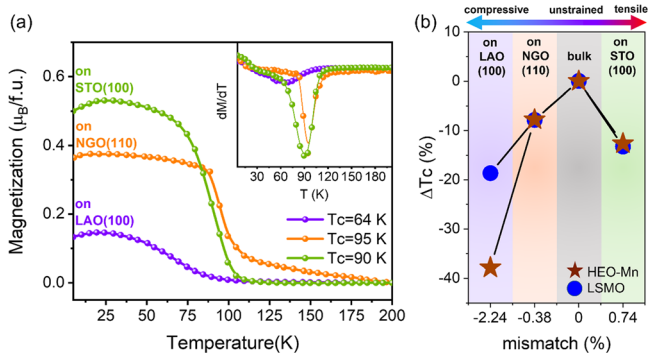

FIG. 5. (a) *In-plane* field cooled (FC) M-T curves of HEO-Mn films deposited under various substrates. The derivative (dM/dT_{FC}) shown in the inset (a) is used for estimating the T_C. (b) Comparison of the change in T_C as a function of lattice mismatch in HEO-Mn vs conventional manganite (LSMO).[23,24]

magnetic state at 105 K, which is further used for comparison with the studied films. In the case of strained HEO-Mn thin films, there are two factors which affects the Mn–O–Mn bond geometry: one is the aforementioned intrinsic non-uniformity resulting in locally varying Mn–O–Mn bonds and the other one is the induced epitaxial strain that is uniform, hence changes the Mn–O–Mn bond geometry in a coherent manner. The fact that the strained HEO-Mn thin films exhibit a single Curie temperature (T_c) illustrates that epitaxial strain dominates over the local fluctuations arising from A-site disorder. Essentially, the Mn–O–Mn bonds appear to have a more uniform alignment, a property attributed to the coherent nature of the epitaxial strain.

We consider the impact of the applied strain on the magnetic critical temperatures by estimating the T_c of the HEO-Mn films from the derivative (dM/dT_{FC}) of the FC M-T curves, as shown in the inset of Fig. 5(a). For the samples deposited on the STO and NGO substrates, which are subjected to a relatively small amount of strain, distinct magnetic transitions are observed. In both cases, the T_C is slightly lower than that of the bulk counterpart, 90 and 95 K for the STO and NGO substrates, respectively. Conversely, the magnetic transition of HEO-Mn on LAO substrate, which occurs about 40 K lower than that of bulk HEO-Mn, is gradual and covers a wide temperature range [inset in Fig. 5(a)]. Significant reduction in the MS also accompanies the lowering of the T_c in the case of films deposited on LAO (as shown in Fig. S3). One of the plausible reasons is that the high degree of induced epitaxial strain starts favoring the antiferromagnetic phase at the expense of the ferromagnetic one resulting in the drop of MS to 1.5 μB/f.u. for the film deposited on LAO.

The variations in the T_c for differently strained HEO-Mn thin films are illustrated in Fig. 5(b). Oxygen stoichiometry and resulting Mn oxidation states have a strong influence on the magnetic properties of manganites. Hence, spectroscopic studies were performed to distinguish the oxygen stoichiometry related effects from the strain mediated ones. X-ray absorption spectroscopy and x-ray emission spectroscopy (Fig. S4) indicated that the Mn oxidation state remains unaltered among the HE-Mn films deposited on NGO, LAO, and STO. This suggests that the changes in T_c observed in the different HE-Mn films studied here are primarily caused by epitaxial strain. For comparison, data from a conventional manganite system ($La_{0.7}Sr_{0.3}MnO_3$, LSMO) with similar lattice parameter ($a_{pc} = 3.87$ Å) deposited on identical substrates with a similar degree of lattice mismatch are superimposed in Fig. 5(b). For clarity, changes in the T_c are presented relative to their bulk counterparts. The response of the T_c to strain is similar in the case of the HEO-Mn on NGO and STO substrates, practically following the behavior of conventional LSMO. In both cases, a small amount of strain (either compressive or tensile), such as that induced by NGO or LAO, causes the T_c to decrease with respect to the bulk. However, a clear outlier in Fig. 5(b) is the marked decrease in T_c (a decrease in −38%) for the HEO-Mn deposited on LAO. The modulation of the IP lattice parameter as a function of the thickness, as indicated by the TEM results (shown in Fig. 4), could be one of the underlying factors. The fact that the Mn–O–Mn bonding angle varies locally remains valid due to the presence of the multiple RE cations (which is true for even HEO-Mn deposited on STO and NGO). However, in the HEO-Mn/LAO case, the coherent straining also varies along the thickness of the film. Hence, across the film thickness, the average IP Mn–O–Mn bond angle changes from one unit cell to the other. The changes in the bond geometry are expected to have a direct impact on the strength of the Mn–O–Mn exchange interactions, which could be manifested in terms of the drastic changes in the T_c. Nevertheless, further studies, especially theoretical, are crucial to confirm the interpretations presented and to understand the reasons, leading to the unique changes in the magnetic properties of heavily strained HEO-Mn deposited on LAO substrate.

In summary, this work demonstrates the deposition of 25 nm thick single crystal orthorhombic $(Gd_{0.2}La_{0.2}Nd_{0.2}Sm_{0.2}Sr_{0.2})MnO_3$ films on cubic-STO (100), orthorhombic-NGO (110), and cubic-LAO (100) substrates to induce varying epitaxial strains. A combination of characterization techniques, at both macro- and nano-scales, clearly demonstrates the phase purity and epitaxy of the HEO-Mn films. The HEO-Mn film on NGO shows superior epitaxial quality, while the strongly strained HEO-Mn film on the LAO substrate exhibits lattice relaxation and significant mosaicity. Even for HEO-Mn/LAO, TEM images display fully coherent film growth at the interface, albeit with a clear variation in the in-plane lattice parameter across the film thickness. The magnetic properties of all the HEO-Mn thin films notably differ from the bulk polycrystalline HEO-Mn. Unlike bulk HEO-Mn, which features two magnetic transitions, all the HEO-Mn thin films exhibit a single magnetic transition. This phenomenon is attributed to the cohesive nature of the epitaxial strain, which leads to a more uniform alignment of the Mn–O–Mn bonds in thin films. Irrespective of the straining strength and type, a decrease in the T_c compared to the bulk is observed in all the HEO films. Importantly, HEO-Mn/LAO exhibits a remarkable lowering of the T_c (−38%). In the HEO-Mn/LAO film, the strong variation of the in-plane lattice parameter across the film thickness, which affects the Mn–O–Mn bond length and geometry, is believed to significantly influence the magnetic double-exchange interactions. Thus, this initial study highlights the potential for manipulating the structure and properties of perovskite manganites via combination of the high entropy design approach and epitaxial strain engineering.

See the supplementary material for the experimental section, full range XRD scans, TEM micrographs for sample deposited on LAO, M-H plots, x-ray absorption spectroscopy, and x-ray emission spectroscopy data.

Z.Z., R.K., and H.H. acknowledge the support from the European Union's Horizon 2020 research and innovation program under the Marie Skłodowska-Curie Grant Agreement No. 861145 (BeMAGIC, MSCA). X.P., M.W., H.H., and A.S. acknowledge the financial support from the National Science Foundation Materials Research Science and Engineering Center program through the UC Irvine Center for Complex and Active Materials (DMR-2011967). A.K.J. acknowledges financial support from the European Union's Framework Program for Research and Innovation, Horizon 2020, under the Marie Skłodowska-Curie Grant Agreement No. 847471 (QUSTEC). A.S. and H.H. acknowledge financial support from the Deutsche Forschungsgemeinschaft (DFG) project HA 1344/43-2. M.W. and X.P. acknowledge the use of facilities and instrumentation at the UC Irvine Materials Research Institute (IMRI) supported in part by the National Science Foundation Materials Research Science and Engineering Center program through the UC Irvine Center for Complex and Active Materials (DMR-2011967). J.L. acknowledges the Fonds der Chemischen Industrie (FCI) for the financial support. J.L. and T.B.

acknowledge the European Synchrotron Radiation Facility (ESRF) for the provision of synchrotron radiation facilities under proposal number MA-6219 (https://doi.esrf.fr/10.15151/ESRF-ES-1550923205) and the assistance from Dr. Sami Juhani Vasala for support in using beamline ID26. We acknowledge support by the KIT-Publication Fund of the Karlsruhe Institute of Technology.

AUTHOR DECLARATIONS

Conflict of Interest

The authors have no conflicts to disclose.

Author Contributions

Zhibo Zhao: Conceptualization (supporting); Data curation (equal); Formal analysis (equal); Investigation (equal); Methodology (lead); Writing – original draft (supporting). **Moaz Waqar:** Data curation (equal); Formal analysis (equal); Investigation (equal); Methodology (equal); Writing – review & editing (supporting). **Arun Kumar Jaiswal:** Data curation (supporting); Formal analysis (supporting); Methodology (supporting); Writing – review & editing (supporting). **Aaditya Rangan Raghavan:** Investigation (supporting); Methodology (supporting). **Dirk Fuchs:** Data curation (supporting); Formal analysis (supporting); Methodology (supporting); Validation (equal); Writing – review & editing (supporting). **Jing Lin:** Formal analysis (supporting); Investigation (supporting); Methodology (supporting). **Torsten Brezesinski:** Formal analysis (supporting); Investigation (supporting); Methodology (supporting). **Subramshu S. Bhattacharya:** Supervision (supporting); Validation (supporting); Writing – review & editing (supporting). **Horst Hahn:** Funding acquisition (lead); Project administration (lead); Supervision (supporting); Writing – review & editing (supporting). **Xiaoqing Pan:** Funding acquisition (equal); Project administration (equal); Resources (equal); Supervision (supporting). **Robert Kruk:** Conceptualization (supporting); Funding acquisition (supporting); Supervision (equal); Visualization (equal); Writing – review & editing (lead). **Abhishek Sarkar:** Conceptualization (lead); Data curation (equal); Formal analysis (equal); Supervision (lead); Writing – original draft (lead); Writing – review & editing (equal).

DATA AVAILABILITY

The data that support the findings of this study are available within the article and its supplementary material.

REFERENCES

[1]A. Sarkar, Q. Wang, A. Schiele, M. R. Chellali, S. S. Bhattacharya, D. Wang, T. Brezesinski, H. Hahn, L. Velasco, and B. Breitung, "High-entropy oxides: Fundamental aspects and electrochemical properties," Adv. Mater. **31**(26), 1806236 (2019).

[2]B. L. Musicó, D. Gilbert, T. Z. Ward, K. Page, E. George, J. Yan, D. Mandrus, and V. Keppens, "The emergent field of high entropy oxides: Design, prospects, challenges, and opportunities for tailoring material properties," APL Mater. **8**(4), 040912 (2020).

[3]S. S. Aamlid, M. Oudah, J. Rottler, and A. M. Hallas, "Understanding the role of entropy in high entropy oxides," J. Am. Chem. Soc. **145**(11), 5991–6006 (2023).

[4]A. Sarkar, B. Breitung, and H. Hahn, "High entropy oxides: The role of entropy, enthalpy and synergy," Scr. Mater. **187**, 43–48 (2020).

[5]J. Dąbrowa, M. Stygar, A. Mikuła, A. Knapik, K. Mroczka, W. Tejchman, M. Danielewski, and M. Martin, "Synthesis and microstructure of the (Co,Cr,Fe,Mn,Ni)$_3$O$_4$ high entropy oxide characterized by spinel structure," Mater. Lett. **216**, 32–36 (2018).

[6]Q. Wang, L. Velasco, B. Breitung, and V. Presser, "High-entropy energy materials in the age of big data: A critical guide to next-generation synthesis and applications," Adv. Energy Mater. **11**(47), 2102355 (2021).

[7]A. Sarkar, L. Velasco, D. Wang, Q. Wang, G. Talasila, L. de Biasi, C. Kübel, T. Brezesinski, S. S. Bhattacharya, H. Hahn, and B. Breitung, "High entropy oxides for reversible energy storage," Nat. Commun. **9**(1), 3400 (2018).

[8]M. Fracchia, P. Ghigna, T. Pozzi, U. Anselmi Tamburini, V. Colombo, L. Braglia, and P. Torelli, "Stabilization by configurational entropy of the Cu(II) active site during CO oxidation on $Mg_{0.2}Co_{0.2}Ni_{0.2}Cu_{0.2}Zn_{0.2}O$," J. Phys. Chem. Lett. **11**(9), 3589–3593 (2020).

[9]R. Banerjee, S. Chatterjee, M. Ranjan, T. Bhattacharya, S. Mukherjee, S. S. Jana, A. Dwivedi, and T. Maiti, "High-entropy perovskites: An emergent class of oxide thermoelectrics with ultralow thermal conductivity," ACS Sustain. Chem. Eng. **8**(46), 17022–17032 (2020).

[10]A. Sarkar, B. Eggert, L. Velasco, X. Mu, J. Lill, K. Ollefs, S. S. Bhattacharya, H. Wende, R. Kruk, R. A. Brand, and H. Hahn, "Role of intermediate 4f states in tuning the band structure of high entropy oxides," APL Mater. **8**(5), 051111 (2020).

[11]N. Sharma, S. Jangid, S. Choudhury, S. K. Mahatha, R. P. Singh, and S. Marik, "Large exchange bias effect and complex magnetism in a tetragonal high entropy spinel oxide," Appl. Phys. Lett. **123**(16), 161901 (2023).

[12]Z. Zhao, A. K. Jaiswal, D. Wang, V. Wollersen, Z. Xiao, G. Pradhan, F. Celegato, P. Tiberto, M. Szymczak, J. Dabrowa, M. Waqar, D. Fuchs, X. Pan, H. Hahn, R. Kruk, and A. Sarkar, "Strain-driven bidirectional spin orientation control in epitaxial high entropy oxide films," Adv. Sci. **10**(27), e2304038 (2023).

[13]V. Strotkötter, O. A. Krysiak, J. Zhang, X. Wang, E. Suhr, W. Schuhmann, and A. Ludwig, "Discovery of high-entropy oxide electrocatalysts: From thin-film material libraries to particles," Chem. Mater. **34**(23), 10291–10303 (2022).

[14]R. Witte, A. Sarkar, R. Kruk, R. A. Brand, H. Wende, and H. Hahn, "High entropy oxides: An emerging prospect for magnetic rare earth transition metal perovskites," Phys. Rev. Mater. **3**, 034406 (2018).

[15]A. R. Mazza, E. Skoropata, Y. Sharma, J. Lapano, T. W. Heitmann, B. L. Musico, V. Keppens, Z. Gai, J. W. Freeland, T. R. Charlton, M. Brahlek, A. Moreo, E. Dagotto, and T. Z. Ward, "Designing magnetism in high entropy oxides," Adv. Sci. **9**(10), 2200391 (2022).

[16]A. R. Mazza, E. Skoropata, J. Lapano, M. A. Chilcote, C. Jorgensen, N. Tang, Z. Gai, J. Singleton, M. J. Brahlek, D. A. Gilbert, and T. Z. Ward, "Hole doping in compositionally complex correlated oxide enables tunable exchange biasing," APL Mater. **11**(3), 031118 (2023).

[17]A. Sarkar, R. Kruk, and H. Hahn, "Magnetic properties of high entropy oxides," Dalton Trans. **50**(6), 1973–1982 (2021).

[18]L. Su, H. Huyan, A. Sarkar, W. Gao, X. Yan, C. Addiego, R. Kruk, H. Hahn, and X. Pan, "Direct observation of elemental fluctuation and oxygen octahedral distortion-dependent charge distribution in high entropy oxides," Nat. Commun. **13**(1), 2358 (2022).

[19]A. Sarkar, D. Wang, M. V. Kante, L. Eiselt, V. Trouillet, G. Iankevich, Z. Zhao, S. S. Bhattacharya, H. Hahn, and R. Kruk, "High entropy approach to engineer strongly correlated functionalities in manganites," Adv. Mater. **35**, 2207436 (2022).

[20]C. W. Huang, W. Ren, V. C. Nguyen, Z. Chen, J. Wang, T. Sritharan, and L. Chen, "Abnormal Poisson's ratio and linear compressibility in perovskite materials," Adv. Mater. **24**(30), 4170–4174 (2012).

[21]Y. Sharma, B. L. Musico, X. Gao, C. Hua, A. F. May, A. Herklotz, A. Rastogi, D. Mandrus, J. Yan, H. N. Lee, M. F. Chisholm, V. Keppens, and T. Z. Ward, "Single-crystal high entropy perovskite oxide epitaxial films," Phys. Rev. Mater. **2**(6), 060404 (2018).

[22]Y. Ogimoto, M. Nakamura, N. Takubo, H. Tamaru, M. Izumi, and K. Miyano, "Strain-induced crossover of the metal-insulator transition in perovskite manganites," Phys. Rev. B **71**(6), 060403 (2005).

[23]F. Tsui, M. C. Smoak, T. K. Nath, and C. B. Eom, "Strain-dependent magnetic phase diagram of epitaxial $La_{0.6}7Sr_{0.33}MnO_3$ thin films," Appl. Phys. Lett. **76**(17), 2421–2423 (2000).

[24]C. Adamo, X. Ke, H. Q. Wang, H. L. Xin, T. Heeg, M. E. Hawley, W. Zander, J. Schubert, P. Schiffer, D. A. Muller, L. Maritato, and D. G. Schlom, "Effect of biaxial strain on the electrical and magnetic properties of (001) $La_{0.7}Sr_{0.3}MnO_3$ thin films," Appl. Phys. Lett. **95**, 112504 (2009).